Proper orthogonal decomposition of thermally-induced flow structure in an enclosure with alternately active localized heat sources

Pallab Sinha Mahapatra[1, 2], Souvick Chatterjee[1, 2], Achintya Mukhopadhyay[1], Nirmal K. Manna[1] and Koushik Ghosh[1]

[1]*Department of Mechanical Engineering, Jadavpur University, Kolkata 700032, India*

[2]*Department of Mechanical and Industrial Engineering, University of Illinois at Chicago, IL 60607, USA*

Abstract

The paper presents the structure of buoyancy-driven flow occurring in an enclosure with two alternately active discrete heat sources. For the analysis of the mixing of the fluid layer and its effect on heat transfer process, the flow information has been presented both in time and spectral domain. The inherent dynamics is also studied using the proper orthogonal decomposition (POD). POD technique is used here to assess the energy content in the different modes and the related coherent structures of flow considering different Rayleigh numbers (Ra=10^3-10^6), switching frequencies (Z^{-1} with Z=0.1-0.8) and air as working fluid of Prandtl number (Pr) of 0.71. The results reveal nonlinear characteristics of hydrodynamics and heat transfer at higher Ra for low frequency. Here, POD helps understanding the flow dynamics from information about the coherent structures of different energy modes.

Keywords: transient natural convection; alternate heating; proper orthogonal decomposition, flow structures

1.0 INTRODUCTION

Researchers have studied natural convection in enclosures for several decades due to its widespread applications, such as cooling of electronic equipment, thermal insulation, solar collector, etc. In contrast to steady-state study of heat transfer, relatively less work is available on the pulsatile heating from the bottom wall of an enclosure. Unsteady heating with a sinusoidal or other form of temperature variation of walls was also studied earlier [1-9]. Although some work has been reported which deal with intermittent heating of enclosures and the consequent flow and thermal dynamics [8], the effect of periodic activation of multiple heat sources in an enclosure has only recently been investigated [10]. This configuration assumes significance in the context of thermally aware scheduling in multi-core processors of modern computers where jobs are allotted to different processors with an objective of minimizing hot spot formation. Although such scheduling is done primarily from considerations of ability of the system to dissipate the generated heat, our recent work [11] shows that alternate activation of two discrete heat sources in a cavity can alter the flow inside the enclosure itself leading to significant heat transfer augmentation. The pronounced effect of the switch-over frequency on heat transfer augmentation motivates a more detailed investigation of the underlying physics. The objective of the present work is to gain insight into the transport phenomena involved from an in-depth study of the fluid flow caused by the buoyancy effect.

The effect of alternately active heating from the bottom of an enclosure on the heat and fluid flow characteristics is assessed in this paper utilizing well-established methodologies. For the analysis of the mixing of the fluid layer and its effect on heat transfer process, the flow information has been presented both in time and spectral domain. The inherent dynamics is also studied using the proper orthogonal decomposition (POD). POD is a powerful decomposition technique for identifying the energetic modes that correlates the physical flow field. POD is extensively used in different thermo fluidic problems [12-15]. Ding et al. [16] used numerical data and highlighted the advantage of generating faster results through POD and used this concept to interpolate results at off-design parameters at a substantially less computational cost. Bleris and Kothare [17] analyzed the dynamics of thermal transience in a micro-system using POD. Data from finite element model (FEM) has been used as an input for this processing technique to test the performance of a controller. Khashehchi et al. [18] used POD on velocity fields generated by particle image velocimetry (PIV) to analyze the instabilities in flow past finned and foamed circular cylinder. The POD methodology was used by different researchers for a host of natural convection problems [19-22]. Podvin and Le Quéré [20] used low-dimensional models for representing chaotic flows in a differentially heated cavity. They observed that before the bifurcation point, the dynamics of the system could be reduced down to two energetic modes, although it is necessary to account for higher modes in the model beyond the bifurcation point. A ten-dimensional model successfully captured the chaotic flow dynamics far away from the bifurcation point. A turbulent Rayleigh-Bénard convection in a square domain was studied by Bailon-Cuba and Schumacher [21]. The low dimensional model based on POD of the velocity and temperature fields and the snapshot of direct numerical simulation (DNS) results were used to describe the temporal evolution of the large-scale mode amplitudes for a particular Rayleigh and Prandtl number. Podvin and Sergent [22] performed the large-eddy simulation (LES) of turbulent Rayleigh-Bénard convection of air in a parallelepiped cavity and used POD to describe the large-scale structures of the flow with their temporal evolution and found out their roles on the convective heat and momentum transfer.

Bae and Hyun [10] showed enhanced heat transfer by systematic changing of the state of the heaters (switching "on" and "off")inside an enclosure. Detailed heat transfer analysis of a case of pulsatile heating using alternately active two heaters in an enclosure is reported in authors' earlier work [11], which revealed the pronounced effect of the switch-over frequency on heat transfer augmentation. Since the transient results of various quantities presented in our earlier work [11] suggest superposition of several energetic modes, the effect of switching frequency on fluid flow pattern inside the enclosure is analyzed using POD technique. The objective of this present work is to extract spatial flow information in terms of coherent structures of different energy modes. In this work, POD snapshot method as has been discussed by Sirovich and Kirby [23] has been utilized and energy content in different modes along with contours of higher modes has been explicitly shown.

The paper is organized as follows: In Sec. 2, overview of the physical system and the CFD simulation are given. The details of POD analysis of the CFD generated flow structure is given in Sec. 3. In Sec. 4, the flow characteristics of the system are discussed with the help of different modal structures, FFT of the eigenmodes and streamfunctions. The POD modes for different pulsation frequencies are shown. Lastly, a conclusion is given in Sec. 5.

2.0 DESCRIPTION OF PHYSICAL SYSTEM AND CFD SIMULATION

The schematic of the enclosure and heaters with their thermal conditions are shown in Fig. 1a, where two alternately active isothermal heaters (temperature T_H) are placed at the bottom wall of the enclosure. The assumption of constant temperature of the heat source is common in the context of electronic cooling e.g., [24]. Adiabatic boundary is assumed on the heater surface when the heater is switched "off". Top wall and non-heated portion of bottom wall are adiabatic while a constant temperature T_C is maintained at the side walls ($T_H > T_C$). The switch-over time period (Z, dimensionless) is defined as the time interval between the consecutive switching "on" (or "off") of a particular heater.

The motion of stagnant confined fluid inside the enclosure is initiated due to density difference when either of the heaters is switched on. The alternate activation of the heaters generates complex dynamics in the flow field. After the initial transience of flow establishment, periodic circulation patterns are evolved consisting of two circulating cells (vortices). The characteristics of evolved oscillatory flow pattern (as shown in Fig. 1b) with the interrupted heating is responsible for transporting heat in the enclosure and found strongly dependent on *Z* and Ra in our earlier study [11]. This is a buoyancy-driven flow and was simulated considering two-dimensional, laminar and incompressible flow within the framework of Boussinesq approximation and assuming rigid and impermeable walls, and no-slip boundary conditions. CFD simulations were carried out using an extremely validated in-house code based on the finite volume method (FVM) and SIMPLE algorithm [25], considering a set of dimensionless conservation equations for mass, momentum and energy as given below.

$$\nabla.\mathbf{V} = 0 \tag{1}$$

$$\frac{\partial \mathbf{V}}{\partial \tau} + (\mathbf{V}.\nabla)\mathbf{V} = -\nabla P + \mathrm{Pr}\,\nabla^2\mathbf{V} + \mathrm{RaPr}\,\theta\,\mathbf{e}_\mathrm{y} \tag{2}$$

$$\frac{\partial \theta}{\partial \tau} + (\mathbf{V}.\nabla)\theta = \nabla^2\theta \tag{3}$$

The last term in Eq. (2) is the buoyancy force acting antiparallel to gravity (g), along the direction of vertical unit vector $\boldsymbol{e}_y$, and is coupled to dimensionless velocity (***V***) and pressure (*P*) terms of Navier-Stokes momentum equation. In above equations, *L* is taken as domain length scale and $\frac{\alpha}{L}$ as the velocity scale where α is the thermal diffusivity of the working fluid. The temperature and physical time are non-dimensionalized by $\theta = (T - T_C)/(T_H - T_C)$ and $\tau = t/(L^2/\alpha)$ respectively.

The simulated stream function (ψ) inside the enclosure is utilized as "inputs" to the POD analysis that explores the underlying flow physics in terms of modal structure and power spectral density (PSD) function. The study is limited for the Rayleigh number ($\mathrm{Ra} = \mathrm{Pr}(g\beta(T_H - T_C)L^3)/\nu^2$) in the range of 10^3 to 10^6 and Prandtl number ($\mathrm{Pr} = \nu/\alpha$) of 0.71, where β and ν are respectively volumetric thermal expansion coefficient and kinematic viscosity of the working fluid.

3.0 POD PROCEDURE

POD executes a linear analysis in terms of optimal basis functions and a fluctuating entity, which can be any flow field data or image intensities from an experiment. In this work, the analysis has been performed on stream function data obtained numerically as described earlier. For this process, the stream functions at all spatial locations (row size, m and column size, n) for a particular time instant are reshaped into a vector (*u*). Such vectors for N successive time instants are arranged in adjacent columns to form a snapshot matrix, U of dimensions mn × N such that:

$$U = \left[u_1, u_2, u_3, \ldots\ldots, u_N\right] \tag{4}$$

In POD, the flow field is decomposed into a set of basis functions (spatial functions, φ) and mode coefficients (temporal functions, *a*) which gives:

$$u(r,t) = \sum_{k=1}^{N_m} a_k(t)\varphi_k(r) \tag{5}$$

where N_m is the finite number of modes and $N \le N_m$ and *r* denotes direction. The snapshot matrix, U is used to calculate the N dimensional symmetric and positive semi-definite temporal correlation matrix *C* given by:

$$C = U^T U \tag{6}$$

The solution of linear eigenvalue problem, $C\sigma^k = \lambda_k \sigma^k$ allows the construction of eigenvectors σ^k (k=1,…,N_m). The symmetry of the correlation matrix demands the eigenvalues λ_k to be real, the magnitude of which provides a measure of the energy content of the corresponding eigenvectors. Hence, the eigenvectors are ordered by the magnitude of their corresponding eigenvalues.

The assumption of the snapshot version of POD used in this analysis is that the spatial eigenfunctions or eigenmodes (φ) are linear combinations of the snapshots with eigenvectors of the temporal correlation matrix as the coefficients such that:

$$\varphi_k(r) = \sum_{n=1}^{N} \sigma_n^k u(r, t_n) \tag{7}$$

which, in matrix representation, implies pre-multiplication of the eigenvectors with the data matrix, U. Thus, the eigenfunctions satisfies spatial orthogonality condition. We normalized the spatial eigenfunctions using their respective norms. The temporal coefficients (a(t))are analytically obtained by projecting the flow fields onto each eigenfunction [16] such that:

$$a_k(t_n) = (u(r, t_n), \varphi_k(r)) \; k = 1,2,,,,N_m; n = 1,....., N \tag{8}$$

The presence of multiple frequencies in a problem generally corresponds to a superposition of frequencies of these modes which is evident from their waveform [26]. In particular, when these modes are exactly out-of-phase with one another, they correspond to a circular structure in the phase space of the corresponding two modes [27]. Certain energy coefficients have been defined in the literature [16] that provide a quantitative estimate of the energy content in the POD modes:

The participating energy coefficient (ξ_n) which represents the fractional energy in n-th mode and the cumulative energy coefficient (η_n) are defined as,

$$\xi_n = \lambda_n / \sum_{n=1}^{N} \lambda_n \tag{9}$$

$$\eta_n = (\sum_{n=1}^{N_m} \lambda_n) / \sum_{n=1}^{N} \lambda_n \tag{10}$$

Here λ_n represents the energy content of the nth mode.

In this work, POD helps to understand the complexities of thermally induced flow phenomenon by studying the different modes.

4.0 RESULTS AND DISCUSSIONS

The heat and fluid flow during natural convection in a square cavity with alternately active heat sources from the bottom of the enclosure as shown in Fig. 1a has been studied numerically for a Prandtl number of 0.71. Detailed heat transfer analysis has been reported in the authors' earlier work [11], and it was found that for a very high pulsation frequency the condition approaches a state of two steadily active heaters. With the increase of the switchover frequency, the thermal boundary layer formation over the active heater changes rapidly and the destruction of the thermal boundary layer leads to the improved heat transfer. At a low Z value or higher frequency, the heaters are being switched "on" and "off" very fast and the system gets less time to respond fully to this sudden alternation so that the effects of both the heaters prevail in a quasi steady manner.

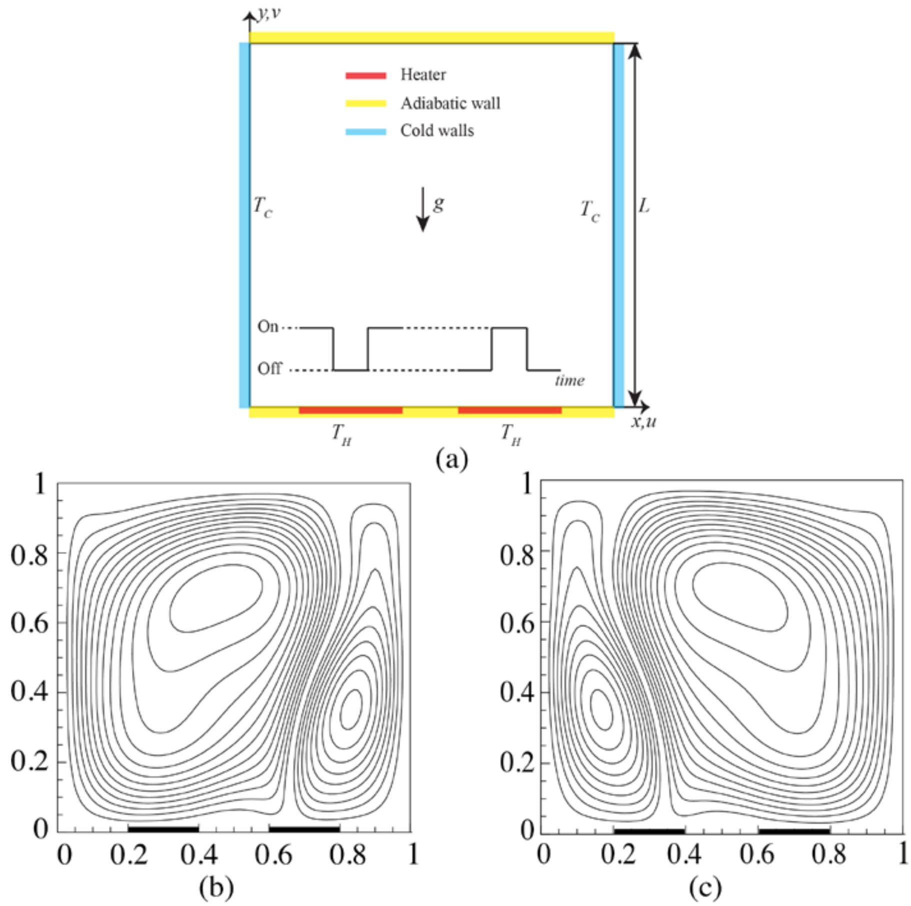

Figure 1: (Color online) (a) Schematic of the computational domain. The vortical structures formed inside the enclosure for Z=0.1 and Ra=10^6 at two different time instants (b) τ =1, 1.1 and (c) τ =1.05.

Two primary vortices are formed due to bottom heating as shown in Fig. 1b. The vortices grow and shrink periodically depending upon the switching frequency of the heaters. At higher Z the inertia of the circulating cell introduces nonlinear effects in the system. It is worth mentioning here that this nonlinearity dies down with the decrease of the convection strength of the circulating cell as Ra decreases. At low Ra of 10^3 periodic characters are observed in all the flow variables with only one dominating frequency of external perturbation whereas, at higher Ra the waveform gets distorted. In this work we used POD to explore the dynamics at higher Ra which shows increased nonlinearity. In POD analysis, the eigenvalues represent the energy content in the corresponding eigenmode. The first eigenmode, denoting the mean non-fluctuating mode, is expected to contain the maximum energy. The fractional energy content is significant until the third mode. The higher modes are primarily contributed by the noise.

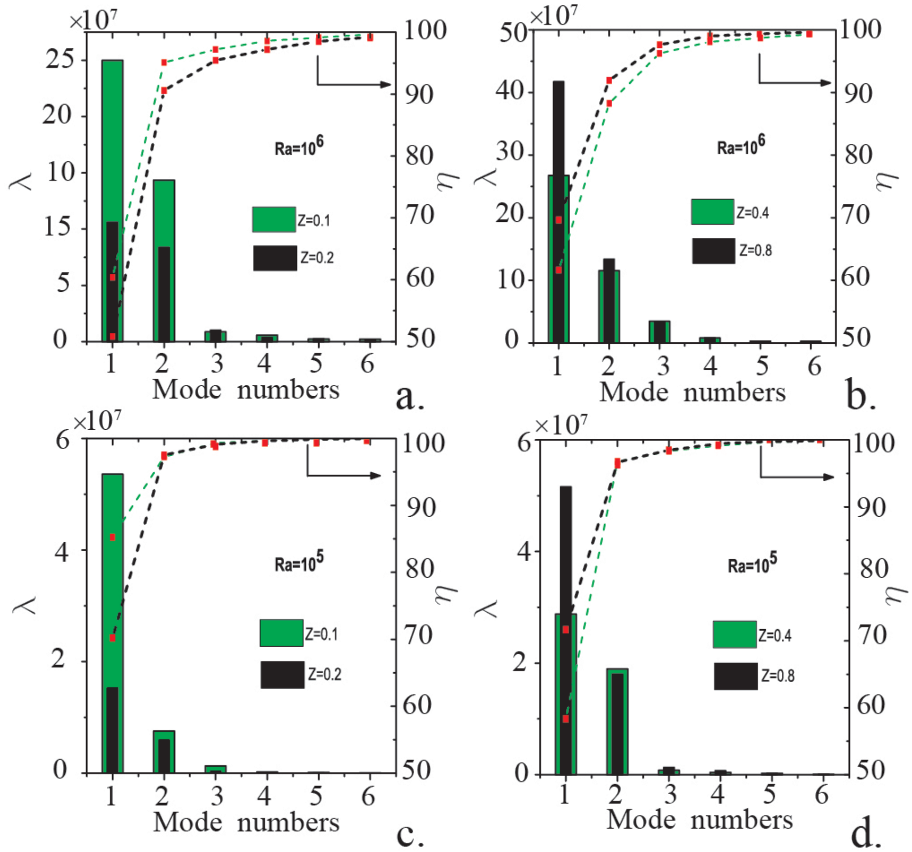

Figure 2: (Color online) Eigenvalues and cumulative energy coefficient for different modes at different Ra and Z. (a) for Ra = 10^6 and Z= 0.1 and 0.2 (b) for Ra = 10^6 and Z= 0.4 and 0.8 (c) for Ra = 10^5 and Z= 0.1 and 0.2 (d) for Ra = 10^5 and Z= 0.4 and 0.8. For all Ra and Z the cumulative energy coefficient is ~100 % after mode 3.

The first six eigenvalues (λ) of the stream function contours, in the descending order of magnitudes, are presented in Fig. 2 for Z = 0.1 to 0.8 at Ra = 10^5 and 10^6. The corresponding cumulative energy coefficient η_n is also shown in the secondary axis of each subfigure along with the eigenvalues. From Fig. 2 it is observed that the cumulative energy reaches ~100 % within first three modes with the first eigenvalue expectedly having the largest magnitude and hence the most participant energy. At Ra=10^6 it alone captures 60.41 % and 50.64 % of the total energy for Z=0.1 and 0.2 respectively. The magnitude of the eigenvalue for Z=0.2 decreases sharply from 1.06×10^8 in the first mode to 1.02×10^7 in the third mode and further to 1.5×10^6 in the sixth mode. Eigenvalue and energy distribution of stream function at Z=0.4 for Ra=10^6 is shown in Fig. 2b. Figure 2b demonstrates that the first eigenvalue has the largest magnitude and the most participant energy, and it alone captures 61.64 % of the total energy. It should be noted that the energy content of the first mode increases 11 % with the increase of Z from 0.2 to 0.4 at Ra=10^6. With the increase of Z the system tends to reach the quasi steady-state situation of single heater placed asymmetrically at the bottom wall of the enclosure. The energy content of the first mode increases with the decrease of Ra. The energy content of the first mode for Ra=10^5 and Ra=10^4 at Z=0.2 are 70.20 % and 87.91 % respectively. As the energy content of the first mode increases significantly with the decrease of Ra, the first mode contains the main contribution of forming the coherent structures. With the decrease of energy content in the eigenmodes, increasingly smaller structures are observed in the higher modes. Similar conclusions have also been drawn by Feng et al. [28] where they observed that the first few modes dominates the global flow field. It should be noted that, at very small Z almost all the energy (>99 %) are contained in the first mode. At Z=0.01 the magnitude of the eigenvalue decreases sharply from 5.69×10^7 in the first mode to 1.06×10^{-7} in the second mode.

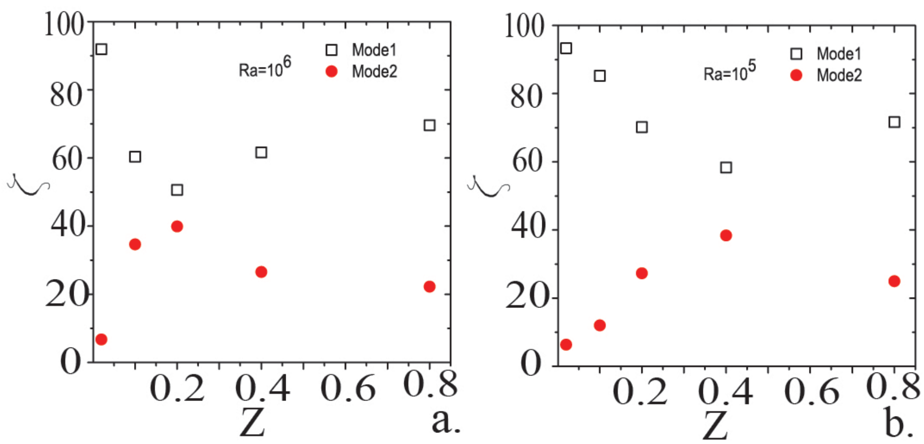

Figure 3: Energy content in different modes for Ra=10^5 and Ra = 10^6. As demonstrated in (a), at Ra= 10^6 the energy content of mode 1 is minimum at Z=0.2 and at the same point the energy content of mode 2 is maximum. For Ra=10^5 as shown in (b), the minimum energy of mode 1 and maximum energy of mode 2 is observed at Z=0.4.

The energy content in the first two energetic modes for different switch-over time period Z is shown in Fig. 3. The energy content in the first mode is minimum and maximum for mode 2 at Z = 0.2 for Ra=10^6. The minimum energy in the first mode at Z=0.2 denotes that the mean strength of the circulating cell is weaker than that of the first mode structure corresponding to Z=0.4. The energy content in the second mode is highest at Z=0.2, which signifies the stronger fluctuating energy distribution through the second mode. A similar point of minimum energy content in mode1 is observed at Z=0.4 for Ra=10^5 (cf. Fig. 3b). Thus, higher modes tend to show dominance at higher Z for lower Ra. For analysis of the modal structures, we concentrate on three Z values for each of Ra=10^5 and 10^6: the period with minimum first mode energy and two of its neighbouring periods.

The first three dominant modes obtained from the streamline data are shown in Fig. 4 for Ra=10^6 and Z=0.1. Eigenmodes with large eigenvalues take the shape of large scale smooth structures. The streamline contours clearly show the presence of two counter rotating vortices at mode 1. At higher frequency (Z≤0.1) the system gets lesser time to respond during alternate heating and the system tends to reach a two active heater situation. The two circulating structures are not symmetric as the energy of mode 2 is also significant (34.7 %). The structure of mode2 further breaks down into smaller structures at higher modes. First three modes contains around 97.2 % of energy where the first mode represents the steady state character of two circulating cells in the domain and the second and the third modes represent the fluctuating modes that transfer the energy from one circulating cell to other. The first three modes show large-scale structures and in the further higher modes the presence of small-scale structures increases. The FFT of the eigenmodes are shown in Fig. 4d. The first dominant frequency is observed in mode 2, which is ~Z^{-1}. At this frequency, mode1 shows the lowest power.

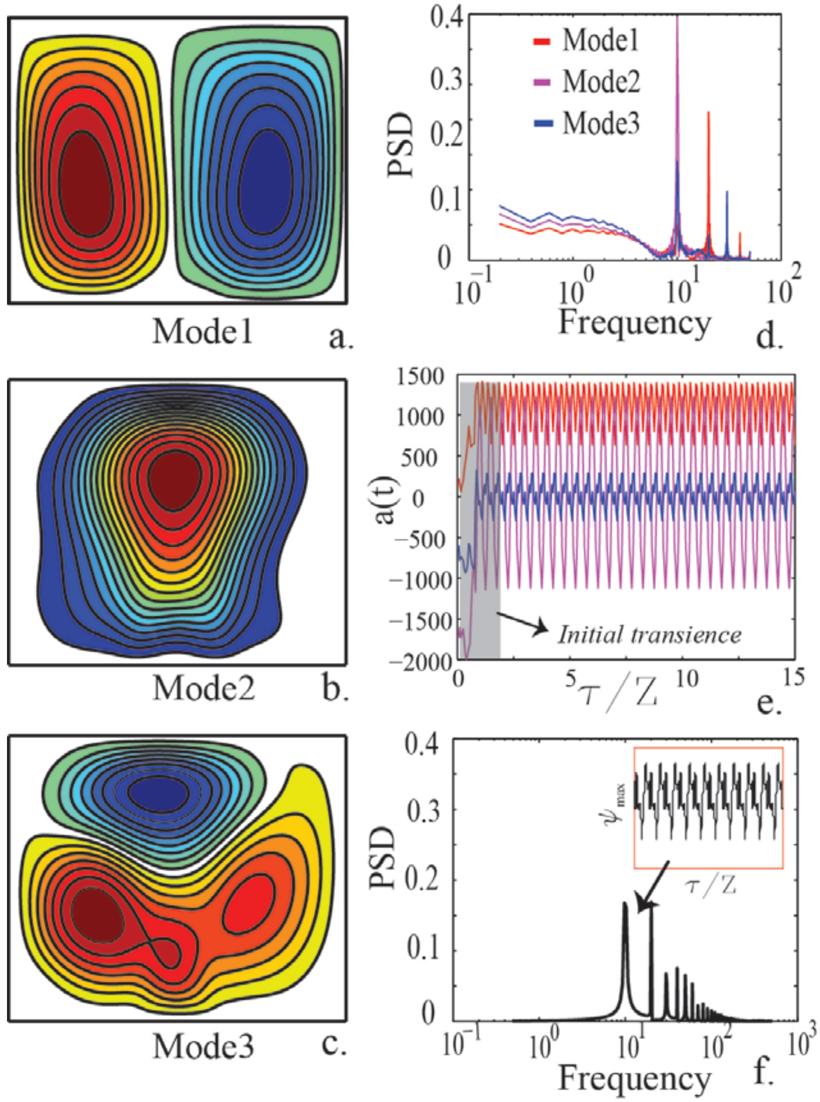

Figure 4: (Color online) Modal structure and FFT of eigenmodes and maximum stream function for Z=0.1 and Ra=10^6. Three modal structures of the eigenmodes are shown in (a), (b) and (c) respectively. In (d) the FFT of the eigenmodes is shown. The power of mode 2 is maximum and this corresponds to the switching frequency ~ Z^{-1}. The temporal coefficients of the three modes are shown in (e). The time series and FFT of maximum stream function is shown in (f).

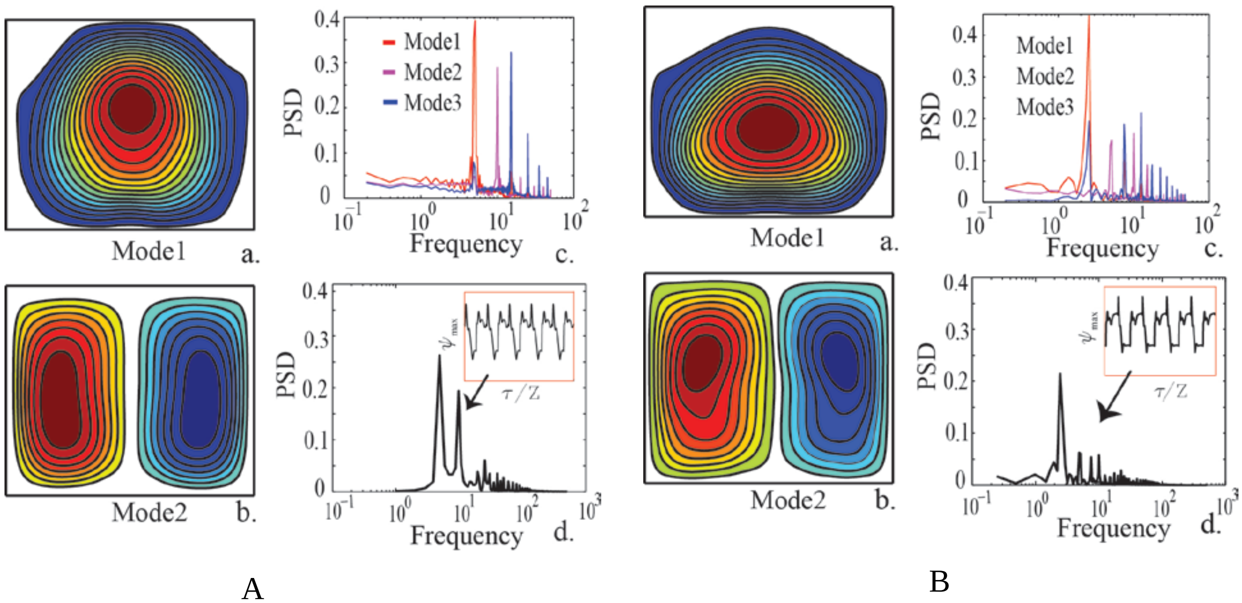

Figure 5: (Color online) Modal structure and FFT of eigenmodes and maximum stream function for (A) Z=0.2 and (B) Z=0.4 for Ra=10^6. Two modal structures of the eigenmodes are shown in (a) and (b) respectively. In (c) the FFT of the eigenmodes is shown. The power of mode 1 is maximum and this corresponds to the switching frequency ~ Z^{-1}. The time series and FFT of maximum stream function is shown in (d).

Higher frequencies are the harmonics of the dominant one. The first mode with two large-scale coherent structures appears at a frequency, which is the first harmonic of the switch-over frequency. Each such structure represents a circulation with a singularity at the center. Since each roll spans approximately half the enclosure, their turnaround time is about half of the single rolls and hence the occurrence of the peak at the first harmonic is physically intuitive. In addition, the first and third modes have one and three circulations showing frequencies that are the fundamental and third harmonic respectively. However, the frequencies of all the modes are harmonics, and their superposition leads to a complex waveform as seen from Fig. 4e. The time series and the FFT of the maximum stream function are shown in Fig. 4f. Since the eigenvalues of the first two modes are of comparable orders of magnitude, the effect of superposition of the two modes is evident in both the waveform (distortion of the waveform) and its FFT (presence of the fundamental and the first harmonic of comparable strength).

At Z=0.2, as shown in Fig. 5c, mode 1 shows one dominant frequency ~ Z^{-1}. Thus, the single structure in the eigenfunction plot (Fig. 5a) of this configuration shows up at this frequency. In mode 2, this structure breaks up into two counter-rotating vortical structures. As in the previous case, the mode with a single roll has the dominant peak ~ Z^{-1} while that of the one with two rolls is the first harmonic of the switch-over frequency. Two such structures in mode 2 further break down into smaller structures at higher modes. First three modes contain around 95 % of energy. The shift of the single structure to the first mode makes it the most dominant power spectrum in the FFT in Fig. 5c and thus this mode shows the dominant frequency of ~ Z^{-1}. The structure of eigenfunctions in mode 3 is similar for Z=0.4 and Z=0.2 for $Ra=10^6$. The large separation in the magnitudes of the first two eigenvalues at Z =0.4 leads to a clear dominance of a single frequency in the FFT of the maximum stream function. On the other hand, at Z =0.1 and Z =0.2, similar orders of magnitude of the first two eigenvalues lead to the existence of strong multiple peaks in the FFT. As shown in our earlier paper [11], at low values of Z, the solution approaches that of an enclosure with two steady discrete heat sources. On the other hand, at high values of Z, the solution moves towards that of a cavity with a single heat source placed asymmetrically. Thus the observation of a single roll structure as the dominant mode at Z = 0.2 and 0.4 and a symmetric double roll structure at Z = 0.1 is consistent with the earlier result [11]. These differences in flow structures have a significant impact on the heat transfer rates as discussed in our earlier paper [11]. However, a detailed discussion is beyond the scope of the present paper.

With the decrease of switching frequency the amplitude as well as the time period of the maximum stream functions increases as in case of lower switching frequency the system gets more time to react to the external perturbation. At very high Z of 0.8, the maximum stream function pattern is almost like a square wave. At Z=0.1 the amplitude of maximum stream functions is small whereas, at Z=0.2 more vigorous fluctuations are observed. At lower Ra due to weak momentum source the fluid flow becomes less intense, and with the increase of switching frequency (lower Z) the maximum stream function shows a sinusoidal variation.

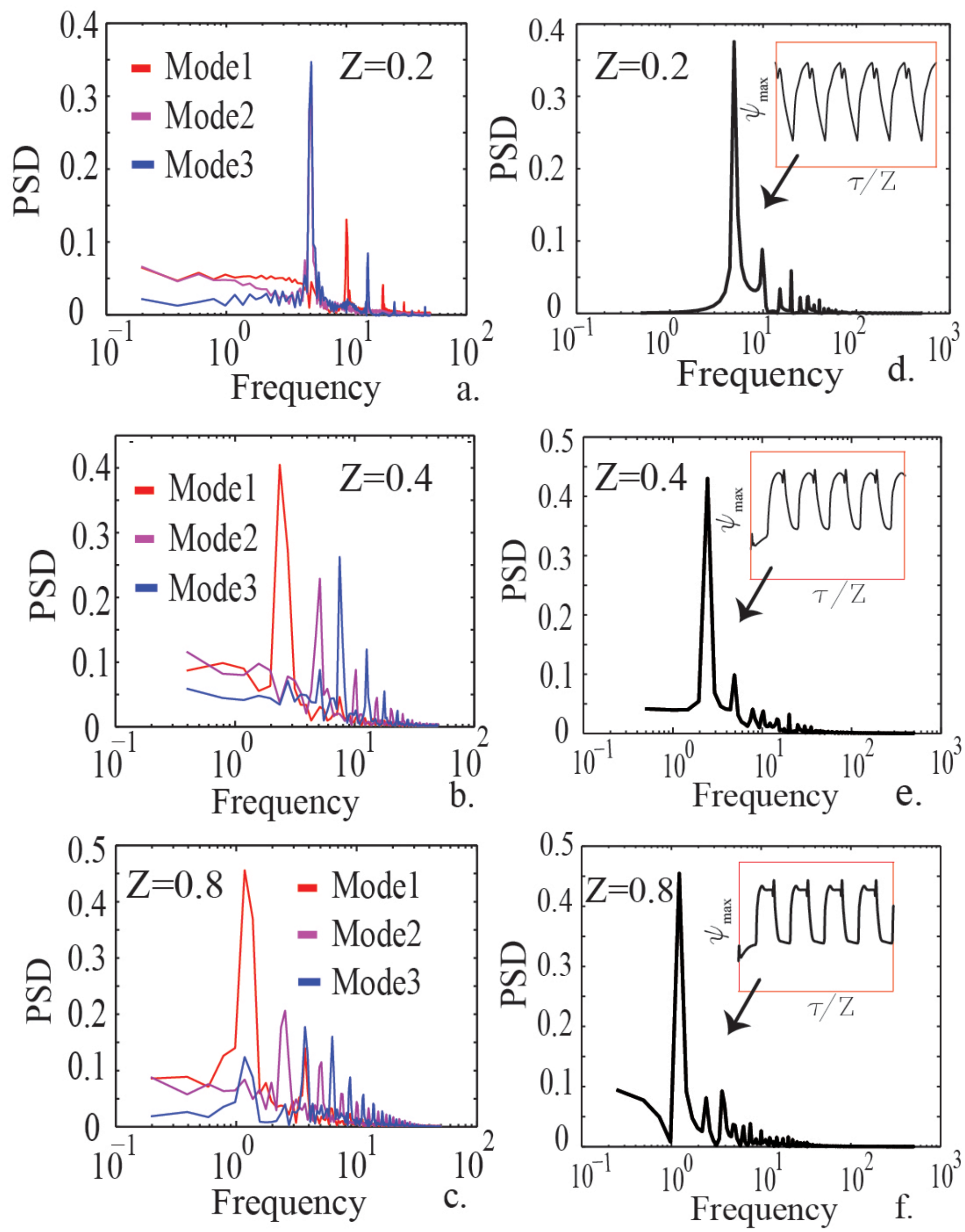

Figure 6: (Color online) FFT of the first three dominant eigenmodes for different Z at Ra=10^5. In (a) the dominant mode is observed for mode 2 at Z=0.2. All the dominant modes frequency corresponds to the switching frequency ~ Z^{-1}. (d, e, f) shows FFT of maximum stream function. The dominant frequency in (d) corresponds to that of mode 3 in (a) while the dominant frequency in (e) and (f) corresponds to that of mode 1 in (b) and (c) respectively.

In Fig. 6 the FFT of first three eigenmodes at different Z for Ra=10^5 is shown. At Z=0.2, mode 2 and 3 have peaks at the frequency Z^{-1}, while mode 1 is least dominant at this frequency. Similar to the dynamics of Z=0.1 and Ra=10^6 (Fig. 4), mode 1 shows two large scale structures and appears at frequency which is the first harmonic of the switch-over frequency. The dominant frequency for mode 1 at Z=0.4, as shown in Fig. 6b, changes to Z^{-1}. Simultaneously, the modal structure also changes. Similar to the Ra=10^6, the modal structure of mode 1 changes from the two rotating cells to one vortical structure from Z=0.4. As in the case of Ra = 10^6, the dominant frequency for mode 1 switches to Z^{-1} at the value of Z for which the fractional energy content of mode 1 is minimum. The complex waveforms and their FFTs obtained from the maximum stream function shown in Fig. 6d, e, f clearly shows superposition of modes 1 and 2. This is particularly evident for Z=0.4 where the first and second eigenvalues are of similar order of magnitude whereas influence of mode 2 is least for Z=0.8 because of its lower eigenvalue. At such higher Z, the square type waveform of the maximum stream function seems to be dominated by the dynamics of mode 1. Further increase of Z does not change the pattern of the dominating modal structure and power. Thus, using three dominant POD modes, the spatio-temporal flow dynamics in the enclosed domain can be clearly understood which proves the power of proper orthogonal decomposition as a modal analysis technique.

5.0 CONCLUSIONS

In this paper, the dynamics of the flow structure caused by natural convection due to alternate heating of two heat sources is analyzed using proper orthogonal decomposition (POD). The heat transfer analysis of the said problem was reported earlier and it was found that heat transfer increases with the increase of pulsation frequency. However, in this work, we show the inherent dynamics of the flow inside the domain using POD and compare the modal dynamics with the temporal variation of maximum stream function obtained from FVM solution.

The energy content in each mode is presented which provides a measure of fluctuations in the flow. A mean non-fluctuating mode has been shown that contains the maximum energy. The first three POD modes contain ~97% energy and hence the dynamics can be completely understood from the analysis of these modes. For each Ra, the temporal dynamics in the domain show interesting variation with the switching frequency. There exists a critical value for this frequency at which mode 1 changes from a structure with two circulating cells to one with single vortical structure. In addition, below this critical frequency (which depends on Ra), mode 1 (with single structure) shows the dominant frequency which is the switching frequency and modes 2 and 3 occur at harmonics. However, increased heat transfer occurring at higher switching frequencies correspond to mode 1 occurring at harmonics with modes 2 and 3 appearing at dominant frequency of the switching frequency. For a lower Ra, the system shows increased non-linearity both in heat transfer and fluid flow only when it gets sufficient time to respond to the external perturbation i.e. at high values of Z. Also at this frequency, the energy content in the first mode shows a minimum, which depends on the strength of the heat source. This implies the increased significance of higher modes in the dynamics. The complex waveform of the stream function showed a temporal dynamics similar to superposition of the modes at switching frequencies where higher modes have energy content comparable to the first mode.

REFERENCES

[1] E.K. Lakhal, M. Hasnaoui, P. Vasseur, E. Bilgen, Natural convection in a square enclosure heated periodically from part of the bottom wall, Numer. Heat Transfer A, 27 (1995) 319-333.

[2] S. Roy, T. Basak, Finite element analysis of natural convection flows in a square cavity with non-uniformly heated wall(s), Int. J. Eng. Sci, 43 (2005) 668-680.

[3] A. Raji, M. Hasnaoui, M. Firdaouss, C. Ouardi, Natural convection heat transfer enhancement in a square cavity periodically cooled from above, Numer. Heat Transfer A, 63 (2013) 511-533.

[4] S. Douamna, M. Hasnaoui, B. Abourida, Two-dimensional transient natural convection in a repetitive geometry submitted to variable heating from below: numerical identification of routes leading to chaos, Numer. Heat Transfer, A, 37 (2000) 779-799.

[5] H.S. Kwak, J.M. Hyun, Natural convection in an enclosure having a vertical sidewall with time varying temperature, J. Fluid Mech., 329 (1996) 65-88.

[6] H.S. Kwak, K. Kuwahara, J.M. Hyun, Resonant enhancement of natural convection heat transfer in a square enclosure, Int. J. Heat Mass Transfer, 4(18) (1998) 2837-2846.

[7] B. Abourida, M. Hasnaoui, S. Douamna, Transient natural convection in a square enclosure with horizontal walls submitted to periodic temperatures, Numer. Heat Transfer, A, 36 (1999) 737-750.

[8] J.L. Lage, A. Bejan, The resonance of natural convection in an enclosure heated periodically from the side, Int. J. Heat Mass Transfer, 36(8) (1993) 2027-2038.

[9] H. Ishida, Y. Takagi, N. Kin, H. Yoshimura, G. Kawahara, Resonant thermal convections in a square cavity induced by heat-flux vibration on the bottom wall, Numer. Heat Transfer A, 58 (2010) 20-40.

[10] J.H. Bae, J.M. Hyun, Time-dependent buoyant convection in an enclosure with discrete heat sources, Int. J. Therm. Sci., 43 (2004) 3-11.

[11] P.S. Mahapatra, N.K. Manna, K. Ghosh, A. Mukhopadhyay, Heat transfer assessment of an alternately active bi-heater undergoing transient natural convection, Int. J. Heat Mass Transfer, 83 (2015) 450-464.

[12] L.-H. Feng, J.-J. Wang, Modification of a circular cylinder wake with synthetic jet: Vortex shedding modes and mechanism, Eur. J. Mech. B Fluids, 43 (2014) 14-32.

[13] R. Blanchard, A. Wickersham, L. Ma, W. Ng, U. Vandsburger, Simulating bluff-body flameholders: on the use of Proper Orthogonal Decomposition for combustion dynamics validation, J. Eng. Gas Turb. Power, (2014).

[14] T.K. Sengupta, S.I. Haider, M.K. Parvathi, G. Pallavi, Enstrophy-based proper orthogonal decomposition for reduced-order modeling of flow past a cylinder, Physical Review E, 91(4) (2015) 043303.

[15] S. Roy, J.-C. Hua, W. Barnhill, G.H. Gunaratne, J.R. Gord, Deconvolution of reacting-flow dynamics using proper orthogonal and dynamic mode decompositions, Physical Review E, 91(1) (2015) 013001.

[16] P. Ding, X.-H. Wu, Y.-L. He, W.-Q. Tao, A fast and efficient method for predicting fluid flow and heat transfer problems, J. Heat Transfer, 130(3) (2008) 032502-032517.

[17] L.G. Bleris, M.V. Kothare, Reduced order distributed boundary control of thermal transients in microsystems, Control Systems Technology, IEEE Transactions on, 13(6) (2005) 853-867.

[18] M. Khashehchi, I.A. Abdi, K. Hooman, T. Roesgen, A comparison between the wake behind finned and foamed circular cylinders in cross-flow, Exp. Thermal Fluid Sci., 52 (2014) 328-338.

[19] A.E. Deane, L. Sirovich, A computational study of Rayleigh–Benard convection. Part 1. Rayleigh-number scaling, J. Fluid Mech., 222 (1991) 231.

[20] B. Podvin, P.L. Quéré, Low-order models for the flow in a differentially heated cavity, Phys. Fluids, 13 (2001) 3204.

[21] J. Bailon-Cuba, J. Schumacher, Low-dimensional model of turbulent Rayleigh-B´enard convection in a Cartesian cell with square domain, Phys. Fluids, 23 (2011) 077101.

[22] B. Podvin, A. Sergent, Proper orthogonal decomposition investigation of turbulent Rayleigh-Bénard convection in a rectangular cavity, Phys. Fluids, 24 (2012) 105106.

[23] L. Sirovich, M. Kirby, Low dimensional procedure for the charaterization of human faces, Journal of the Optical Society of America a-Optics Image Science and Vision, 4(3) (1987) 519-524.

[24] Q.-H. Deng, G.-F. Tang, Y. Li, A combined temperature scale for analyzing natural convection in rectangular enclosures with discrete wall heat sources, Int. J. Heat Mass Transfer, 45 (2002) 3437-3446.
[25] S.V. Patankar, Numerical heat transfer and fluid flow, Hemisphere, Washington, DC, 1980.
[26] K. Shaafi, S. Vengadesan, Heat Transfer Characteristics of Flow over a Circular Cylinder with an Upstream Control Rod in Wall Vicinity, Numer. Heat Transfer A, 65(11) (2014) 1044-1068.
[27] V. Durgesh, R.C. Semaan, J.W. Naughton, Revealing unsteady flow structure from flow visualization images, Eur. Phys. J. Spec. Top., 182(1) (2010) 35-50.
[28] L.H. Feng, J.J. Wang, C. Pan, Proper orthogonal decomposition analysis of vortex dynamics of a circular cylinder under synthetic jet control, Phys. Fluids, 23 (2011) 014106.